PDE-Based Deconvolution with Forward-Backward Diffusivities and Diffusion Tensors

Martin Welk, David Theis, Thomas Brox, and Joachim Weickert

Mathematical Image Analysis Group,
Faculty of Mathematics and Computer Science, Bldg. 27,
Saarland University, 66041 Saarbrücken, Germany
{welk, theis, brox, weickert}@mia.uni-saarland.de
http://www.mia.uni-saarland.de

Abstract. Deblurring with a spatially invariant kernel of arbitrary shape is a frequent problem in image processing. We address this task by studying nonconvex variational functionals that lead to diffusion-reaction equations of Perona–Malik type. Further we consider novel deblurring PDEs with anisotropic diffusion tensors. In order to improve deblurring quality we propose a continuation strategy in which the diffusion weight is reduced during the process. To evaluate our methods, we compare them to two established techniques: Wiener filtering which is regarded as the best linear filter, and a total variation based deconvolution which is the most widespread deblurring PDE. The experiments confirm the favourable performance of our methods, both visually and in terms of signal-to-noise ratio.

1 Introduction

In many application contexts, image acquisition leads to blurred images. Blurring is caused e.g. by motion of objects and/or camera during the recording, from defocussing or from specific errors in the optics of the camera. It is therefore desirable to devise methods how to sharpen – to deblur – images. A variety of different approaches has been proposed in the literature which differ greatly in the assumptions made about the image and the blurring process.

An important case of image blurring is convolution with a fixed kernel. This type of space-invariant blurring is especially found when defocussing and optical errors or translatory motion of the camera have caused the blurring.

Under ideal conditions, convolution could be reverted by convolving with an inverse kernel that could, e.g., be computed via the Fourier domain. However, taking the reciprocal of the Fourier transform of some kernel always leads to an unbounded function that needs to be cut at some frequency; moreover, for other than very simple kernels (like Gaussians), zeroes occur which introduce poles into the inverse. For these reasons, a pseudo-inverse is used. By a slight extension of this idea, one obtains Wiener filtering which relies essentially on a regularisation

R. Kimmel, N. Sochen, J. Weickert (Eds.): Scale-Space 2005, LNCS 3459, pp. 585–597, 2005.

of the inversion operation [16, 7]. These linear approaches give reasonable results but the cut-off of high frequencies introduces characteristic oscillatory artifacts (Gibbs-like phenomena) that cannot be avoided by any linear approach [2].

In the case of blurring by Gaussian convolution the special relation between Gaussian convolution and linear diffusion also makes methods based on stabilised inverse diffusion a possible choice [9].

Another class of methods aims at so-called blind deconvolution in which the kernel is not known a priori but is reconstructed simultaneously with the sharpened image. Obviously, assumptions on the image are inevitable here, otherwise the problem is principally underdetermined. A favourable way to encode a-priori assumptions on the image is the use of a variational framework [17]. Variational blind deconvolution has been investigated in [1]. This approach combines deconvolution with segmentation. The convolution kernels are restricted to Gaussians. In the second part of [1], the combination of deconvolution with a known (not necessarily Gaussian) kernel with segmentation is discussed.

The ill-posedness of all deblurring problems makes it reasonable to involve any available a-priori knowledge in the reconstruction process. Methods for deblurring with known kernels are therefore not made superfluous by blind deconvolution techniques; their better understanding can even support the development of blind deconvolution methods.

In this article, we describe PDE-based approaches for deblurring in case of convolution with a space-invariant kernel. We do not make specific assumptions on symmetry of the kernel, instead, our method is designed to work even for fairly irregularly shaped kernels. Our approach is motivated first by a variational model for deconvolution. The involved variational problem is solved via a diffusion–reaction equation where the diffusivity is linked to the regulariser. While total variation (TV) regularisation is a common choice in the literature, we investigate the nonconvex regularisation which leads to forward-backward diffusivity. By generalising to diffusion-reaction PDEs which are no longer associated with variational formulations, we can also include anisotropic diffusion tensors in our study. Experiments show that improvements over established deblurring techniques can be achieved by these methods. Since the non-uniqueness of steady states plays an important role, the treatment of the diffusion weight is a central issue. We present a strategy to avoid unwanted solutions.

We also discuss problems occurring at image boundaries which are caused by the admission of kernels without particular symmetries. Note that many deconvolution methods discussed in the literature restrict the shape of the kernel, e.g. to Gaussians with principal axes parallel to the image boundaries, or motion blurs in directions parallel to the image boundaries. The specific symmetries of such kernels make the treatment of boundaries considerably easier.

We proceed as follows. In Section 2, we discuss linear deconvolution methods. Section 3 then describes a variational deblurring model and derives our basic deblurring PDE. Boundary conditions and the choice of the regularisation parameter are discussed separately. Section 4 is dedicated to extensions of the

basic model. These include the continuation strategy and the introduction of anisotropic diffusivities. Experiments are presented in Section 5.

Related Work. Deblurring problems have attracted the attention of computer vision researchers for a long time, and numerous publications exist on this and related topics. Variational approaches to deconvolution with total variation (TV) regularisation have been investigated e.g. by Marquina and Osher [8] for non-blind, and Chan and Wong [6] for blind deconvolution, or recently Bar, Sochen, and Kiryati [1] which addresses both classes of problems. TV regularisation in image restoration has earlier been studied by Rudin, Osher, and Fatemi [12], see also [10]. A variational approach to blind deconvolution with more general regularisation has been presented by You and Kaveh [17].

Research on existence, uniqueness, and stability of solutions for these and related problems can be found in the work by Bertero, Poggio, and Torre [3]. Continuation strategies have been considered for non-convex variational problems in visual reconstruction by Blake and Zisserman [4] and more specifically in the context of total-variation based denoising by Chan, Chan and Zhou [5].

2 Linear Models

We assume that we have an image f which is the result of convolving the original (sharp) image u with some kernel h and superposing some additive noise n,

$$f(x, y) = (u * h)(x, y) + n(x, y) \; .$$

Assume first that the noise n can be neglected. By Fourier transform, the equation then goes into

$$\hat{f} = \hat{u} \cdot \hat{h} \; .$$

If h is known, one could in principle divide $\hat{f}$ by $\hat{h}$ to restore $\hat{u}$ and thereby u. However, this *inverse filtering* procedure faces the problem that in general $\hat{h}$ will possess zeroes. These represent frequencies which are deleted by blurring with h and must therefore not be present in a noise-free blurred image. But still $\hat{h}$ is close to zero in the vicinity of its zeroes, and, even if it has no zeroes, for high frequencies. But in frequency ranges where $|\hat{h}|$ is small, even minimal amounts of noise are tremendously amplified, rendering the procedure extremely unstable.

The simplest approach to handle this difficulty is the *pseudo-inverse filtering* which eliminates frequencies for which $\hat{h}$ is smaller than some threshold H. A more advanced regularisation of inverse filtering is *Wiener filtering* [16] which replaces $\hat{h}^{-1}$ by $\hat{h}^{-1} \, |\hat{h}|^2 \, / (|\hat{h}|^2 + H^2)$ such that we obtain

$$\hat{u} = \frac{1}{\hat{h}} \cdot \frac{|\hat{h}|^2}{|\hat{h}|^2 + H^2} \cdot \hat{f} \; .$$

This filter displays better stability than pseudoinverse filtering. It has properties of a band-pass and is therefore even well-suited to deal with moderate noise.

All deconvolution methods described up to here are linear methods which allow for efficient implementations via Fourier transforms. However, all of them

display characteristic, shadow-like artifacts particularly near edges and also near the image boundaries depending on the boundary conditions used. As proven in [2–p. 119pp.], linear methods cannot avoid these artifacts. Further improvements can therefore be achieved only with nonlinear methods.

3 The Basic Deblurring PDE

3.1 Variational Motivation

Deconvolution of an image can be achieved by minimising the energy functional

$$E(u) = \int_{\Omega} (h * u - f)^2 + \alpha \Psi(|\nabla u|^2)\, \mathrm{d}x \; . \tag{1}$$

The first summand in the integral – the data term – is the square error of the reconstruction of the blurred image from the deblurred image candidate. This data term arises naturally in the deconvolution context and is also used in the variational blind deconvolution models in [17, 1]. The second summand – the smoothness term or regulariser – uses a monotonically increasing function $\Psi : \mathbb{R}_0^+ \to \mathbb{R}$ to enforce the smoothness of the deconvolved image.

Note that an unregularised energy consisting only of the data term already has the original image as a global minimiser. Unfortunately, this minimum is by far not unique since the data term is in general not strictly convex. If the Fourier transform of h has zeroes, then contributions of the corresponding frequencies may be added to u without changing the data term. Even if $\hat{h}$ has no zeroes, it is very small for e.g. high frequencies. Contributions from such frequencies hardly influence the data term. Hence, the data term cannot effectively suppress artifacts like those encountered for linear methods. The smoothness term is needed to reduce these ambiguities. In the case of a strictly convex regulariser Ψ, the energy E as a whole might even be convex and the minimum therefore unique.

Solutions of our variational problem satisfy the Euler-Lagrange equation

$$0 = \tilde{h} * (h * u - f) - \alpha \operatorname{div} \left(\Psi'(|\nabla u|^2) \nabla u \right) \; .$$

Here $\tilde{h}$ denotes the mirror-kernel $\tilde{h}(x, y) := h(-x, -y)$. A gradient descent leading for $t \to \infty$ to a minimiser of E is given by

$$\partial_t u = -\tilde{h} * (h * u - f) + \alpha \operatorname{div} \left(g(|\nabla u|^2) \nabla u \right) \; , \tag{2}$$

a diffusion–reaction equation where the diffusion term with diffusivity $g(s^2) = \Psi'(s^2)$ is related to the regulariser in the energy functional. This PDE can be solved numerically, in the simplest case by an explicit discretisation.

3.2 Choice of the Diffusivity

An important point in determining the properties of the deconvolution process is the choice of the diffusivity g. The simplest case, the constant diffusivity

$g(s^2) = 1$ which corresponds to Tikhonov regularisation $\Psi(s^2) = s^2$, tends towards an over-smoothed deblurring result because high gradients at edges of the reconstructed image are penalised over-proportionally. Moreover, in this case the whole deconvolution method is again linear and suffers from the artifacts described in the previous section.

Total variation (TV) diffusivity $g(s^2) = 1/|s|$, mostly in its regularised form $g(s^2) = 1/\sqrt{s^2 + \varepsilon^2}$, is a popular choice (see [6, 8, 1]), particularly since it enforces piecewise constant results and therefore encourages sharp edges in the image. We therefore include TV diffusivity in our experiments.

Another interesting choice in isotropic nonlinear diffusion models is the Perona–Malik diffusivity $g(s^2) = (1 + s^2/\lambda^2)^{-1}$ that is related to the nonconvex regulariser $\Psi(s^2) = \lambda^2 \ln(1 + s^2/\lambda^2)$, see [11, 14]. Note that the smoothness energy $\Psi(|\nabla u|^2)$ is no longer convex in this case. It is therefore expected that depending on the initial conditions different solutions are obtained.

To reduce the noise sensitivity of isotropic Perona–Malik diffusion (see [14, 13]) it can be stabilised by using a Gaussian-smoothed gradient ∇u_σ in the diffusivity argument, turning the diffusion expression into $\operatorname{div}(g(|\nabla u_\sigma|^2)\,\nabla u)$. Though this stabilised Perona–Malik diffusivity can easily be used in our diffusion–reaction equations (which in this case cease to be gradient descents for energy functionals), experiments indicate that it bears no clear advantages in this case.

3.3 Boundary Conditions

For solving the diffusion–reaction equations of type (2), suitable boundary conditions must be specified. In many diffusion-based image processing methods, reflecting Neumann boundary conditions work well because they guarantee conservation properties as well as a continuous extension of the image at its boundary. Periodic boundary conditions for a rectangular domain lead instead to a wrap-around of image information between opposite boundaries; moreover, they introduce discontinuities which often entail artifacts in the processed image.

Unfortunately, the usage of reflecting boundary conditions for deconvolution with space-invariant kernels is bound to fail if the kernel is not symmetric w.r.t. the image boundary directions because reflected parts of the image would be blurred with a reflected kernel, violating the model assumptions. Since periodic boundary conditions are compatible with any shift-invariant blur, without imposing symmetry constraints on the kernel, we use periodic boundary conditions or modifications of them.

A chief disadvantage of periodic boundary conditions are the discontinuities introduced at the image boundaries. These lead to strong artifacts near the image boundaries. To mitigate these artifacts as well as the undesired wrap-around of image information in the deblurring with periodic boundary conditions, the image can be extended continuously to a larger image with equal grey-values at opposing boundaries. Periodic boundary conditions then no longer introduce discontinuities, and the wrap-around influences mostly the amended parts of the image. Since the assumptions of our deblurring model are still violated near

the image boundaries, boundary artifacts are reduced but not perfectly eliminated.

For quality measurements in our experiments, we therefore arrange a special setting. We start by extending the sharp test image via horizontal and vertical reflection to quadruple size. Periodic extension of this larger image is equivalent to reflecting extension of the original image. Now the large image is blurred in a periodic setting (i.e. with the left boundary wrapping over into the right one etc.) with the irregular kernel. The resulting image has lost the symmetry of the original larger image. In deblurring this image, we use again periodic boundary conditions. While this approach cannot be used in real deblurring applications where the blurring process is not subject to our control, its advantage is that it admits a measurement of the deblurring quality, e.g. in terms of signal-to-noise ratio, without including discontinuity and boundary artifacts which would dominate the total result otherwise. By doing so, we ensure that the model assumptions are met everywhere, at the cost of making this boundary treatment unsuitable for naturally blurred images.

3.4 Choice of the Diffusion Weight

The extreme ill-posedness of the problem makes the choice of the diffusion weight a difficult problem. We discuss this for the deblurring processes which minimise a variational functional. In absence of noise, the non-regularised energy consisting only of the data term is minimised by the correct solution. However, the data term is insensitive to certain perturbations (those being annihilated by convolution with h), preventing in general the solution to be unique. The diffusion–reaction equation (2) in this case turns into a fixed-point equation without diffusion part.

Assume now the energy is made convex by a suitable regulariser such that a unique solution exists. Even if the weight of the regularisation (and thus of the diffusion) is very small, it is practically only the regularisation term which chooses the solution among those which cannot be discriminated by the smoothness term. As a consequence, even a small diffusion weight can drive the solution far away from the true unblurred image, leading to a deblurring result which heavily depends on the type of regulariser (hence, diffusivity) used.

Particularly with nonconvex regularisers and the corresponding forward–backward diffusivities, the existence of multiple steady states of the deblurring process constitutes another issue. The solution which is really obtained depends heavily on the initial conditions. When using the blurred image as initialisation with small diffusion weight, similar artifacts as for linear deblurring methods evolve. Large diffusion weights, on the other hand, induce an over-smoothing and loss of small-scale details in the image.

3.5 Numerical Implementation

In order to solve equation (2) numerically, finite difference discretisations are used for the diffusion term as well as for the left-hand side. The simplest way to

do so is to use a forward difference for $\partial_t u$ and central differences from the old time step for the diffusion term. Denoting by τ the time step size and by Δx, Δy the spatial step sizes in x, y direction, we are led to the explicit scheme

$$\begin{aligned}\frac{u_{ij}^{k+1} - u_{ij}^{k}}{\tau} &= -R_{ij}^{k} + \tfrac{\alpha}{2\Delta x}((g_{i+1,j}^{k} + g_{ij}^{k})(u_{i+1,j}^{k} - u_{ij}^{k}) - (g_{ij}^{k} + g_{i-1,j}^{k})(u_{ij}^{k} - u_{i-1,j}^{k})) \\ &\quad + \tfrac{\alpha}{2\Delta y}((g_{i,j+1}^{k} + g_{ij}^{k})(u_{i,j+1}^{k} - u_{ij}^{k}) - (g_{ij}^{k} + g_{i,j-1}^{k})(u_{ij}^{k} - u_{i,j-1}^{k}))\end{aligned}$$

where the diffusivity $g(|\nabla u|^2)$ (or stabilised $g(|\nabla u_\sigma|^2)$) is discretised by

$$g_{ij}^{k} = \Psi'\left(\left(\frac{u_{i+1,j}^{k} - u_{i-1,j}^{k}}{\Delta x}\right)^2 + \left(\frac{u_{i,j+1}^{k} - u_{i,j-1}^{k}}{\Delta y}\right)^2\right)$$

and R_{ij}^{k} discretises the reaction term $\tilde{h} * (h * u - f)$ at pixel (i, j) and time $k\tau$.

The discretisation of the reaction term poses a difficulty. Since it contains convolutions, its direct computation in each time step would be extremely costsome, even taking into account that $\tilde{h} * h$ can be precomputed once for all time steps. Note that R_{ij}^{k} is computed via the Fourier domain. Though this still requires one DFT (or FFT for suitable image size) and one inverse transform per time step, computing time is considerably reduced for kernels with large support.

4 Extensions

4.1 Continuation Strategy for Optimisation

It has been explicated that the deblurring model is ill-posed, i.e., it reveals not only several local optima, but may even have multiple global optimum solutions that do not depend continuously on the initial data. Consequently, the gradient descent often does not yield the original image as solution, but some other steady state which can be significantly different. In most cases it contains a rather huge amount of oscillatory structures not present in the original data.

A remedy for this ill-posedness has been the supplement of a regulariser to the energy functional. This regulariser introduces the a-priori knowledge that smooth solutions should be preferred. However, despite the usefulness of non-quadratic regularisers which allow for discontinuities in the solution, the negative consequence of the regularisation is a result that is smoother than the original image, since not the complete amount of blurring is reversed by the process.

Actually, there is no regularisation necessary for the model to yield the original image as an optimum solution of the energy. Even the opposite is true: just in the case *without* regularisation the model has the original image as one of the optimum solutions. The regularisation must only be introduced in order to guide the gradient descent towards one out of several optima that shows the least oscillatory behaviour.

Since the regularisation primarily serves as guidance for the optimisation process, the proposed alternative approach continuously reduces the amount of regularisation during optimization. Instead of considering only one energy functional with a fixed amount of regularisation, a cascade of functionals is taken into account. Starting with a rather large amount of regularisation, this amount is reduced from one member of the cascade to the next, and finally leads to the energy functional without any regularisation. The first members of the cascade prefer smooth solutions and therefore may yield good initialisations close to the smoothest optimum of the next version with less regularisation. On the other hand, the later members of the cascade tend more and more to solve the original deblurring problem without regularisation and therefore yield sharper results. This way, one finally runs into an optimum of the functional without regularisation, yet choosing a specific optimum that is smooth. In most cases this optimum is not exactly the original image (it is often still too smooth), yet it is supposed to be closer to this image than the solutions one obtains without this continuation strategy, i.e. either with a fixed amount of smoothness or without any regularisation.

4.2 Anisotropic Model

An improved reconstruction of edges can further be achieved by substituting the isotropic diffusivity g with an anisotropic diffusion tensor $D(\nabla u_\sigma)$. In our model, we use $D(\nabla u_\sigma) = g(\nabla u_\sigma \nabla u_\sigma^{\mathrm{T}})$ where the Perona–Malik diffusivity g is applied to the symmetric matrix $\nabla u_\sigma \nabla u_\sigma^{\mathrm{T}}$, as usual, by letting g act on the eigenvalues and leaving the eigenvectors unchanged [14]. The resulting equation

$$0 = \tilde{h} * (h * u - f) - \alpha \operatorname{div}(D(\nabla u_\sigma)\nabla u)$$

is not the gradient descent for an energy because of the smoothed gradient. However, this smoothing is inevitable in order to have true anisotropy.

5 Experiments

To illustrate and validate the methods described in the preceding sections, we show experimental results obtained with two test images and two different convolution kernels, Fig. 1. One is a banana-shaped blob with irregularly distributed

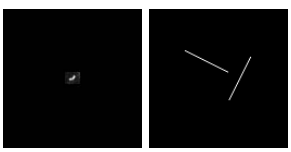

Fig. 1. Convolution kernels. **Left:** Banana-shaped kernel. **Right:** Discontinuous kernel consisting of two line-shaped components

Fig. 2. Left to right: Photograph, 480×640 pixels. – Blurred with banana-shaped kernel. – Deblurred by diffusion–reaction method with Perona–Malik diffusivity, $\lambda = 5$, $\alpha = 0.001$, 1000 iterations. – Photograph blurred with discontinuous kernel. – Deblurred by diffusion–reaction method with Perona–Malik diffusivity, $\lambda = 1$; the continuation strategy was used with two steps for the diffusion weight: 2400 iterations with $\alpha = 0.01$ followed by 2400 iterations with $\alpha = 0$

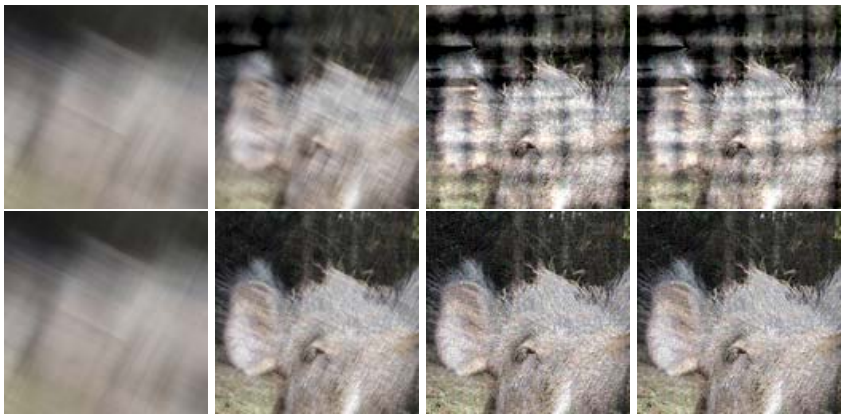

Fig. 3. Deblurring of a detail of the photograph from Fig. 2 with different boundary treatment. **Left to right:** Photograph detail blurred with discontinuous kernel. – Linear deblurring by Wiener filter. – Diffusion–reaction deblurring with TV diffusivity. – Diffusion–reaction deblurring with Perona–Malik diffusivity. **Top row:** Continuous periodic extrapolation of the blurred image (realistic method). While details are well reconstructed, shadow-like boundary artifacts affect the overall quality. **Bottom row:** Same with special setting to suppress boundary artifacts. The image was extended by reflection to four times its original size *before* blurring. This quadruple-size blurred image was then blurred and deblurred with periodic continuation

intensity. This comes close to the blurring of photographs taken with bad illumination and moving camera and objects. The second convolution kernel is discontinuous; it is assembled from two line-shaped parts which are similar to motion blurs. It has been selected as an example of a very challenging kernel.

The first test image used in Figs. 2 and 3 is a photograph with many small-scale details. In fact, this is a colour image to which our diffusion–reaction equations were adapted in the straightforward way with channel coupling. This pro-

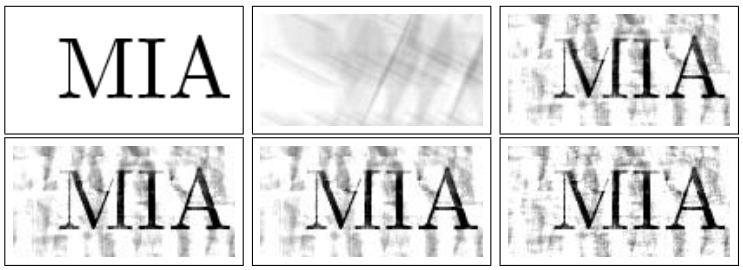

Fig. 4. Top left: Grey-value test image. **Top middle:** Blurred with discontinuous kernel. **Top right:** Linear deblurring by Wiener filter, boundary treatment by continuous extrapolation. **Bottom left:** Diffusion–reaction deblurring with TV diffusivity and continuation strategy (2 levels). **Bottom middle:** Same with Perona–Malik diffusivity. **Bottom right:** Same with anisotropic diffusion tensor

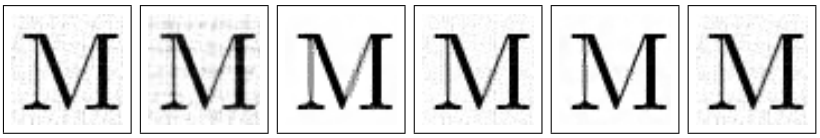

Fig. 5. Detail from deblurred grey-value images, with boundary artifacts suppressed by special test setting. **Left to right:** Linear filtering. – Unregularised variational model. – Perona–Malik, constant diffusion weight. – Perona–Malik followed by nonregularised iteration (two-step continuation strategy). – Perona–Malik, continuation strategy with 10 steps. – Anisotropic diffusion–reaction, continuation strategy with 10 steps

cedure is well-established in nonlinear diffusion literature [14]. The second test image used in Figs. 4 and 5 is a grey-value image of three print letters. It differs from the first image by its composition of fairly homogeneous regions.

In Fig. 2 we blur the first test image with both kernels and restore it by diffusion–reaction deblurring with Perona–Malik diffusivity. For the discontinuous kernel, we also use the continuation strategy in a simple form with one positive α followed by a fixed-point iteration with $\alpha = 0$. Excellent deblurring quality is achieved for the banana kernel (despite its irregularity) while for the discontinuous kernel some shadow-like boundary artifacts are observed.

In Fig. 3, a more detailed comparison of deblurring algorithms is presented for a detail from the photograph blurred with the discontinuous kernel, including Wiener filter as an example of linear deblurring, diffusion–reaction filtering with TV, and Perona–Malik diffusivity. Here we also demonstrate the use of our special test setting to avoid boundary artifacts in quality measurements.

Results for the grey-value test image are shown in Fig. 4. Here, we concentrate on the discontinuous kernel. Besides the methods mentioned above we show also diffusion–reaction deblurring with anisotropic diffusion tensor which performs particularly well for this type of strongly segmented images.

Fig. 5 shows a detail of our grey-value test image to demonstrate the improvements made by anisotropic diffusion tensors and continuation strategy. Pure

Table 1. SNR (dB) for deblurring with the discontinuous kernel. First values: specific test setting for boundary conditions, second values: with continuous extrapolation

	Wiener filtering	Diffusion–reaction, Perona–Malik	Diffusion–reaction, TV diffusivity
Letters	15.6 / 7.1	18.4 / 7.3	17.1 / 7.2
– with contin. strategy		19.3 / 7.4	19.2 / 7.1
Photograph detail	15.9 / 9.4	14.9 / 6.0	14.3 / 5.9

Perona–Malik deblurring reduces oscillatory artifacts quite well but smears thin lines while the fixed-point iteration with $\alpha = 0$ restores many details but generates artifacts similar to those of linear deconvolution. The continuation strategy combines a better restoration of details with a reasonable suppression of artifacts. Even in its simplest form with two steps it bears a clear improvement; more steps lead to further enhancement. The sharpness of edges is further improved by using the anisotropic diffusion tensor.

In Table 1 we compile measurements of the signal-to-noise ratio (SNR)

$$\mathrm{SNR}(v,u) = 10 \log_{10} \frac{\mathrm{var}(u)}{\mathrm{var}(u-v)} \,\mathrm{dB}$$

where u is the original image and v the deblurring result. Throughout the measurements Perona–Malik deblurring tends to slightly better SNR than deblurring with TV diffusivity. However, not always do SNR measurements reflect sufficiently well visual judgement. For the photograph, e.g., the Wiener filter performs better than diffusion–reaction deblurring in terms of SNR. On the other hand, Fig. 3 clearly reveals the superiority of diffusion–reaction deblurring.

6 Conclusions and Ongoing Work

In this paper we have developed diffusion–reaction based deconvolution methods with forward–backward diffusivities motivated from non-convex regularisation. We have established a continuation strategy for the control of the diffusivity weight that allows to combine the suppression of artifacts provided by large diffusion weights with the good reconstruction of details that is typically achieved with small diffusion weights. We have further extended our algorithm by introducing an anisotropic diffusion tensor which allows for a further enhancement of edges in the deblurring process. The favourable performance of the algorithms even for severely blurred images and irregularly shaped kernels has been demonstrated visually and by signal-to-noise ratio measurements.

Ongoing work is dedicated to improvements in the numerical efficiency of our deblurring algorithms, e.g. by utilising additive operator splitting schemes (see [15]). We also work on improving the treatment of boundaries to reduce artifacts even in the restoration of severely blurred images. Because of the observed discrepancies between SNR measurements and visual quality judgement, the development of more adequate quality criteria is a further issue.

References

1. L. Bar, N. Sochen, N. Kiryati. Variational pairing of image segmentation and blind restoration. In T. Pajdla, J. Matas, editors, *Computer Vision – ECCV 2004,* vol. 3022 of *Lecture Notes in Computer Science,* pages 166–177, Berlin, 2004, Springer
2. M. Bertero and P. Boccacci. *Introduction to Inverse Problems in Imaging.* IoP Publishing, Bristol, 1998.
3. M. Bertero, T. A. Poggio, and V. Torre. Ill-posed problems in early vision. *Proceedings of the IEEE*, 76(8):869–889, Aug. 1988.
4. A. Blake and A. Zisserman. *Visual Reconstruction.* MIT Press, Cambridge, MA, 1987.
5. T. Chan, R. Chan, and H. Zhou. A continuation method for total variation denoising problems. In F. Luk, editor, *Proceedings of the SPIE Conference on Advanced Signal Processing Algorithms,* vol. 2563 of *Algorithms, Architectures, and Implementations,* pages 314–325, San Diego, 1995
6. T. F. Chan and C. K. Wong. Total variation blind deconvolution. *IEEE Transactions on Image Processing*, 7:370–375, 1998.
7. R. C. Gonzalez and R. E. Woods. *Digital Image Processing.* Addison–Wesley, Reading, second edition, 2002.
8. A. Marquina, S. Osher. A new time dependent model based on level set motion for nonlinear deblurring and noise removal. In M. Nielsen, P. Johansen, O. F. Olsen, and J. Weickert, editors, *Scale-Space Theories in Computer Vision*, volume 1682 of *Lecture Notes in Computer Science*, pages 429–434. Springer, Berlin, 1999.
9. S. Osher and L. Rudin. Shocks and other nonlinear filtering applied to image processing. In A. G. Tescher, editor, *Applications of Digital Image Processing XIV*, volume 1567 of *Proceedings of SPIE*, pages 414–431. SPIE Press, Bellingham, 1991.
10. S. Osher, L. Rudin. Total variation based image restoration with free local constraints. *Proceedings of the IEEE ICIP*, 31–35, Austin, 1994
11. P. Perona and J. Malik. Scale space and edge detection using anisotropic diffusion. *IEEE Transactions on Pattern Analysis and Machine Intelligence*, 12:629–639, 1990.
12. L. I. Rudin, S. Osher, and E. Fatemi. Nonlinear total variation based noise removal algorithms. *Physica D*, 60:259–268, 1992.
13. J. Weickert. A review of nonlinear diffusion filtering. In B. ter Haar Romeny, L. Florack, J. Koenderink, and M. Viergever, editors, *Scale-Space Theory in Computer Vision*, volume 1252 of *Lecture Notes in Computer Science*, pages 3–28. Springer, Berlin, 1997.
14. J. Weickert. *Anisotropic Diffusion in Image Processing.* Teubner, Stuttgart, 1998.

15. J. Weickert, B. M. ter Haar Romeny, and M. A. Viergever. Efficient and reliable schemes for nonlinear diffusion filtering. *IEEE Transactions on Image Processing*, 7(3):398–410, Mar. 1998.
16. N. Wiener. *Extrapolation, Interpolation and Smoothing of Stationary Time Series with Engineering Applications.* Cambridge (Mass.), 1949, The MIT Press
17. Y.-L. You and M. Kaveh. Anisotropic blind image restoration. In *Proc. 1996 IEEE International Conference on Image Processing*, volume 2, pages 461–464, Lausanne, Switzerland, Sept. 1996.